JET–P(98)45

L-G Eriksson et al

Theoretical Analysis of ICRF Heating in JET D-T Plasmas

JET–P(98)45

Theoretical Analysis of ICRF Heating in JET D-T Plasmas

L-G Eriksson, M Mantsinen[1], V P Bhatnagar, A Gondhalekar, C Gormezano, P Harbour, T Hellsten[2], J G Jacquinot, H Jäckel, K D Lawson, C Lowry, E Righi[3], G Sadler, B Schunke, A Sips, M Stamp, D F H Start.

JET Joint Undertaking, Abingdon, Oxfordshire, OX14 3EA,
[1]Also at Association Euratom-TEKES, Helsinki University of Technology, Finland.
[2]Royal Institute of Technology, S-10044 Stockholm, Sweden..
[3]The NET Team, Garching, Germany.

Preprint of a Paper accepted for publication in Nuclear Fusion

December 1998

ABSTRACT

A number of experiments with heating of deuterium-tritium (D-T) plasmas using waves in the ion cyclotron range of frequencies (ICRF) have been carried out at the Joint European Torus (JET). The results of these experiments have been analysed by comparing experimentally measured quantities with results of numerical simulations. In particular, four scenarios have been examined: (1) heating of minority (~5–20%) deuterons at the fundamental ion cyclotron frequency, $\omega = \omega_{cD}$; (2) second harmonic heating of tritium, $\omega = 2\omega_{cT}$; (3) fundamental minority heating of ^{3}He with a few percent of ^{3}He, and (4) second harmonic heating of deuterium, $\omega = 2\omega_{cD}$. An important aim of the analysis is to assess if the present understanding of the ICRF physics is adequate for predicting the performance of ICRF in D-T plasmas. In general good agreement between experimental results and simulations is found which increases the confidence in predictions of the impact of ICRF heating in future reactors. However, when a relatively high deuterium concentration was used in the $\omega = \omega_{cD}$ scenario, discrepancies are observed. In order to increase confidence in the simulations, we have studied the sensitivity of the simulation results to various plasma parameters.

Subject classification: G2, Ti; G5, Ti; F3, Ti.

1. INTRODUCTION

Heating with waves in the ion cyclotron range of frequencies (ICRF) is one of the main heating methods envisaged for bringing ITER [1] plasmas to thermonuclear temperatures. ICRF heating has been extensively used on existing large scale experiments and has proved effective. ICRF heating of deuterium-tritium (D-T) plasmas, with scenarios relevant for a reactor, has recently been tested in TFTR [2,3] and in a wider frequency range at JET. In JET ICRF heating was used both in high-performance discharges in combination with neutral beam injection [4,5] and in steady-state ELMy H-mode plasmas with ICRF heating alone. For a review of the experimental ICRF-only JET results see Start *et al.* [6,7]. In this paper we present a theoretical analysis of these JET results. We have simulated the impact of ICRF heating on the plasmas, and compared measured and calculated quantities, such as the non-thermal neutron rates. The theoretical analysis is important for assessing whether the present theoretical understanding of the ICRF physics is adequate for predicting the performance of ICRF heating in reactors.

There are several scenarios for ICRF heating of D-T plasmas. The JET ICRF system has therefore been designed for operation in a wide frequency range (23–56 MHz). As a consequence, most of the ICRF heating scenarios relevant for D-T plasmas can be tested. The most favoured scenarios are second harmonic heating of tritium ($\omega = 2\omega_{cT}$) and heating of minority deuterons (10–30%) at the fundamental ion cyclotron frequency ($\omega = \omega_{cD}$). Both have been tested recently, the latter for the first time ever [7]. Furthermore, experiments with ^{3}He minority heating in D-T plasmas have been carried out. In this scenario both ^{3}He minority ions and tritons absorb ICRF power since the ^{3}He cyclotron frequency is equal to the second harmonic triton

frequency. Experiments with second harmonic heating of deuterium and fundamental minority heating of residual hydrogen ($\omega_{cH} = 2\omega_{cD}$) were also carried out, especially in neutral beam heated high performance JET plasmas. Here the experiments carried out in ICRF-only D-T plasmas are analysed. The main features of the analysed discharges are summarised in Table 1.

Table 1 ICRF heating schemes, ICRF powers, antenna frequencies, magnetic fields and tritium concentrations for the discharges analysed in the present paper.

Pulse	heating scheme	P_{ICRF} (MW)	f (MHz)	B_{tor} (T)	$n_T/(n_T+n_D+n_H)$ (%)
43015	$\omega = \omega_{cD}$	6	28.5	3.7	91
42792	$\omega = \omega_{cD}$	5	28.5	3.7	89
42772	$\omega = \omega_{cD}$	4	28.5	3.7	85
42753	$\omega = 2\omega_{cT}$, no ^{3}He puff	8	37.0	3.7	60
42754	$\omega = 2\omega_{cT}$, with ^{3}He puff	8	37.0	3.7	65
41679	$\omega = 2\omega_{cD}$	7	42.5	2.7	60

The ICRF heating scenario currently envisaged as standard for ITER is second harmonic heating of tritium, $\omega = 2\omega_{cT}$. The advantage of the scenario is its applicability to 50:50 D-T plasmas. However, the polarisation at $\omega = 2\omega_{cT}$ in a D-T plasma is not particularly favourable, which together with the absorption being a finite Larmor Radius (FLR) effect tends to lead to weak absorption on the tritons in plasmas with low to moderate temperatures and densities. Another consequence of the absorption being a FLR effect is that high energy tritons tend to interact more effectively with the wave field than tritons with low energies. This can lead to a tail on the triton distribution function with a small number of very energetic tritons. Since these energetic tritons have energies well above the peak of the D-T fusion cross section (around 100 keV), the non-thermal component of the neutron rate is expected to be relatively low. Furthermore, many of the energetic tritons have energies well above the critical velocity for equal electron and ion heating via collisions [8]. Consequently, collisional power transfer from the tritons to the electrons is expected to be significant. In fact, power transfer to the electrons often dominates in low-density, low-temperature plasmas. This situation, which can prevail during the start-up phase in ITER, is undesirable since predominant ion heating would improve the performance during the start-up phase. However, second harmonic heating of tritium in ITER can provide adequate ion heating if the RF-power is applied slightly off-axis and an appropriate route to ignition is followed [9].

According to theoretical expectations, the $\omega = \omega_{cD}$ scenario should give rise to significantly better ion heating and non-thermal fusion yield than the $\omega = 2\omega_{cT}$ scenario. This is

because the interaction in velocity space is more uniform for heating at the fundamental ion cyclotron frequency, i.e. also low energy ions are efficiently accelerated by the ICRF waves. In addition, the damping strength on the deuterons is normally fairly good. However, the $\omega = \omega_{cD}$ scenario is not suitable for a 50:50 D-T plasma, which is a disadvantage. In fact, the best performance in JET was obtained with $n_D/(n_D + n_T) \sim 10\%$. Furthermore, the cyclotron frequency of deuterons is equal to that of alpha particles. Hence, undesired absorption of the RF-power by the alpha particles will take place.

Another option for improving the ion heating is to add a few percent of ^{3}He ions to a plasma with $\omega = 2\omega_{cT} = \omega_{c^3He}$. In this case ^{3}He fundamental minority heating will, according to calculations presented in this paper, absorb a substantial part of the RF-power. The power absorbed by the ^{3}He ions can be efficiently transferred via collisions to the background ions since the critical velocity for ^{3}He ions is quite high and the tail formed on the ^{3}He distribution function is normally moderate.

To simulate ICRF heating, the power deposition calculation using a wave propagation code needs to be combined with a Fokker-Planck code calculating the distribution function(s) of the resonating ion species. Furthermore, since the wave propagation and absorption depends on the velocity distribution function(s) of the resonating ions, the calculation should be self-consistent. This is particularly important for the $\omega = 2\omega_{cT}$ scenario where the absorption is an FLR effect and hence very sensitive to the details of the triton distribution function. In principle one can combine a full wave code such as LION [10] or ALCYON [11] with a two or three dimensional Fokker-Planck code, see e.g. Refs [12,13]. However, due to long execution times on present computers, such code packages are not very practicable. In order to analyse a large number of discharges, simplified models are required. We have used the PION code [14,15] for the present analysis. This code is based on simplified models, and is therefore relatively fast. In general the code gives results that agree well with more complete modelling. However, there are of course certain limitations of the code. In particular, the modelling of mode conversion is not expected to be adequate in cases where mode conversion plays a major role.

Previously, the PION code has been used to analyse various heating scenarios in JET [14,16], and has been found in many cases to provide an adequate description of the ICRF physics on JET. Furthermore, it was used extensively before the experiments with D-T plasmas to predict the influence of various parameters on the performance of ICRF heating. On the whole these predictions turned out to be correct.

The outline of this paper is as follows. In Sec. 2 we give a brief description of the PION code, and the data used in the analysis. In Sec. 3 the results from the analysis of $\omega = \omega_{cD}$ heating in JET are presented, and in Sec. 4 discharges with second harmonic heating of tritium and ^{3}He minority heating are analysed. In Sec. 5 an analysis of the second harmonic deuterium heating is presented. Finally in Sec. 6 the results are summarised, and their implications for ICRF heating in D-T reactor plasmas are discussed.

2. NUMERICAL METHODS

2.1 Description of the model

The major part of the analysis presented in this paper has been done with the PION code [14,15]. PION is a time-dependent code which calculates the ICRF power deposition and the velocity distribution function(s) of the resonating ions. At the beginning of each time step the power deposition is calculated. The output is then used to calculate time evolution of the distribution function(s) with a Fokker-Planck model. The output from the Fokker-Planck calculation at the end of the time step is used in the power deposition at the next time step, and the whole procedure is repeated until the end of the calculation.

In the power deposition calculation the launched wave is Fourier decomposed in the toroidal direction. The power deposition is then calculated for each toroidal mode number according to the model described in Refs [17,18]. This model has been partly obtained by analysing results from the full wave code LION [10]. Consequently, the calculated deposition profiles are generally in good agreement with those given by the LION code. Owing to FLR effects, the absorption strength depends on the distribution function of the resonating ions. In order to take this into account, the dielectric tensor components used in the power deposition calculation are updated, using results from the Fokker-Planck calculation, at the beginning of each time step according to the procedure described in Ref. [15]. The power going to mode conversion is subtracted from the coupled power by treating the absorption layer locally as in planar geometry and calculating the mode conversion as resonance absorption with the Budden formula [19].

The distribution function(s) of the resonating ions are calculated with a time-dependent 1D Fokker-Planck equation [14]. Effects due to finite orbit widths are taken into account by assuming that the fast ions have turning points close to the cyclotron resonance (i.e. where $\omega \approx n\omega_{ci}$) and then averaging the collision coefficients over the resulting orbits. Furthermore, the averaged square parallel velocity, which is used to determine the Doppler broadening of the cyclotron resonance in the power deposition calculation, is obtained from an *ad hoc* formula given in Ref. [20].

Effects due to finite orbit widths played an important role during second harmonic heating of tritium in JET as very energetic tritons were created. For the magnetic field and the plasma current used in the discharges ($B_T \approx 3.7$ T, $I_p \approx 3.3$ MA and $R_{maj} \approx 3$ m) particle orbit calculations show that tritons with energies above about 5 MeV are so energetic that they intersect the wall. To take this into account, a particle loss term that removes tritons above 5 MeV was included in the PION code. Since spatial transport of the thermal part of the resonating ion distribution function is not modelled in the PION code, which uses experimentally measured density profiles as input, a source term of thermal particles has been added to maintain the measured density of tritons.

Since the influence of sawtooth crashes on the neutron emission profile has been found to be significant [7], a model for redistribution of fast ions during sawtooth crashes [21] has been

included in the code. This redistribution model assumes the fast ions to follow field lines and is therefore only applicable to medium fast ions. Consequently, it has been applied to cases where the calculated tails have been found to be moderate. In the model reconnection can be treated in different ways, including the Kadomtsev reconnection. However, differences in the simulation results between the different ways to treat reconnection have been found to be small [21].

In the experiments short tritium neutral beam injection pulses (beam blips) were used for diagnostic purposes. During second harmonic heating of tritium some ICRF power is expected to be absorbed by these tritium beam ions. To take this into account, the beam package implemented [22] in the PION code was used in these cases.

2.2 Input data

All the input data used in the PION code are taken from the JET experimental data base. In the simulations presented in this paper the electron densities and temperatures are those measured by a Lidar Thomson scattering diagnostic. Unless otherwise stated, the ion temperature profiles are given by a charge exchange spectroscopy measurement at the times of diagnostic tritium beam blips. To estimate the ion temperature profile at other times, the profile at a beam blip is scaled with the ion temperature measured around $r/a \approx 0.4$ by the X-ray crystal spectrometer. Since the radius of the ion temperature measurement by an X-ray crystal spectrometer is outside the sawtooth inversion radius (located e.g. in $\omega = \omega_{cD}$ discharges around $r/a \approx 0.35$), sawtooth relaxation is not seen in the modelled ion temperature. Furthermore, the tritium, deuterium and hydrogen concentration are taken to be spatially constant, estimated from the high-resolution measurements of the T_α, D_α, and H_α lines at the plasma edge. In the simulations of discharges with ^{3}He gas puff, the ^{3}He concentration, estimated from the charge exchange spectroscopy at the time of the beam blips, is assumed to be constant in time and space.

3. ANALYSIS OF DEUTERIUM MINORITY HEATING

3.1. Simulation of the neutron rate

In the best performing discharge with $\omega = \omega_{cD}$ heating a steady-state Q of 0.25 was achieved with 6 MW of ICRF power alone. An overview of this discharge is displayed in Fig. 1. A comparison between the measured and simulated D-T fusion reaction rate for the discharge is shown in Fig. 2. Here, results are shown from simulations both with and without taking the redistribution of fast ions at the sawtooth crashes into account. As can be seen in Fig. 2, very good agreement between the simulation and the experiment is obtained, especially with the sawtooth redistribution model. The calculated non-thermal contribution is as high as 90%, which is, as discussed above, due to the fact that at the fundamental cyclotron frequency the waves interact strongly with low-energy deuterons. This leads to a significant increase of non-thermal deuterons in the 100 keV range where the D-T fusion cross-section peaks.

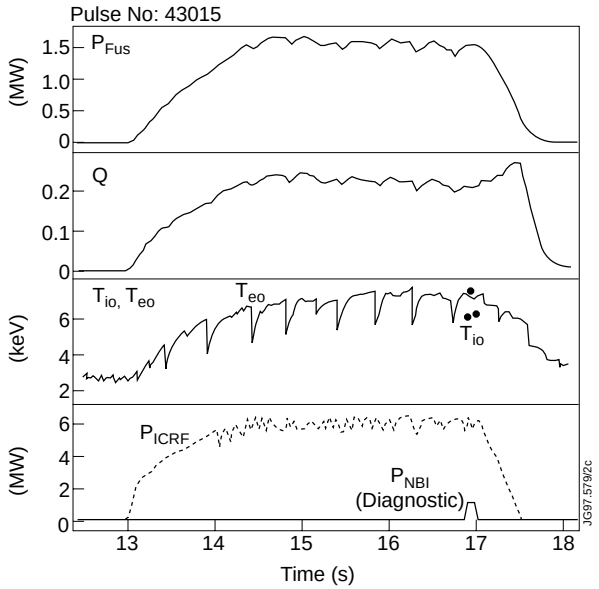

Fig. 1 An overview of the best performing discharge with $\omega = \omega_{cD}$ heating.

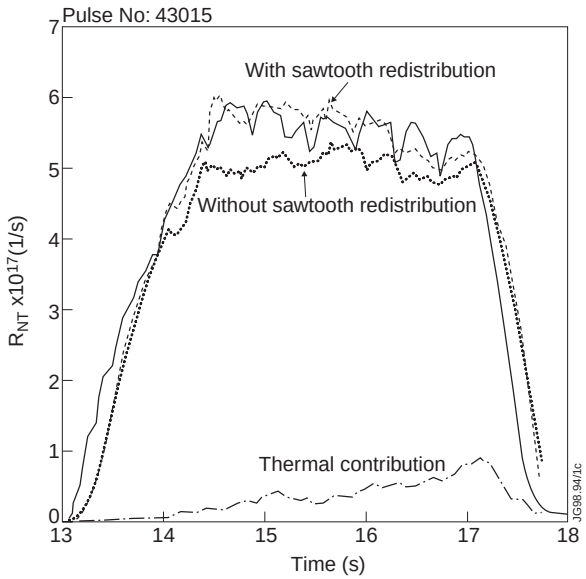

Fig. 2 Measured and simulated D-T fusion reaction rate for the best performing discharge with $\omega = \omega_{cD}$ heating. Simulation results are shown both with and without sawtooth redistribution.

As can be seen in Fig. 2, there are slight discrepancies between the simulations and measurements both in the rise phase and in the decay phase of the neutron rate. The most likely reason for the discrepancies in the rise phase is that at the beginning of the discharge the central deuteron concentration is somewhat smaller than the one measured at the plasma edge (another possibility could of course be that the power deposition is initially somewhat more peaked than predicted by PION). The discrepancies during the decay phase are attributed to a sawtooth crash at t = 17.07 s. For a short period around this time point, the electron temperature measurements used in the simulations did not take any data, and therefore the sawtooth crash at t = 17.07 s, which is visible in other diagnostics, has not been taken into account.

The total neutron yield in the discharges with $\omega = \omega_{cD}$ heating is only slightly affected by the sawtooth crashes. However, measurements of the neutron emission profile show that the sawtooth crashes strongly affect the neutron emission profile [7]. A typical example is shown in Fig. 3 by Start *et al.* [7]. The time-evolution of the neutron emission profile after a sawtooth crash given by PION for this particular discharge is shown in Fig. 3. (Note that

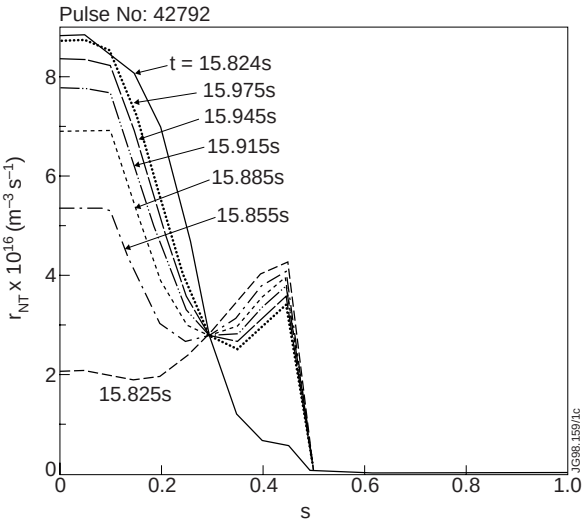

Fig. 3 Time-evolution of the calculated neutron emission profile between t = 15.824 s and t = 15.975 s for discharge 42792 with $\omega = \omega_{cD}$ heating. Here $s = \sqrt{\psi/\psi_a} \approx r/a$, ψ is the poloidal flux and r/a is the normalised minor radius.

the abrupt decrease of the neutron rate around $s = 0.5$ is an artefact of the modelling. In reality, small amounts of spatial diffusion will smooth out the profiles.) The simulated neutron emission profile, which before the crash is peaked as shown at $t = 15.824$ s, becomes hollow at the sawtooth crash as is shown at $t = 15.825$ s. At the sawtooth crash the simulated neutron emission decreases by about 70% in the plasma centre, which is in good agreement with the experiment. The recovery time of the central neutron emission in the simulation is about 30 ms, which is also consistent with the experiments. Note that the neutron profile just before a sawtooth crash is somewhat more peaked than the experimental neutron profile in Fig. 3 in Ref. [7]. Simulations using the Monte Carlo ICRF code FIDO [13], which solves an orbit averaged Fokker-Planck equation and includes effects of finite orbit width and radial transport of the resonating ions (neo-classical and RF-induced), show that the broader profile can be explained by radial transport of the resonating ions.

3.2 Power partition

In addition to absorption on deuterons, the fast wave power is damped on other species, and a fraction can also be mode converted to an ion Bernstein wave. In the steady phase of the discharge the calculations show that about 70% percent of the power is absorbed on deuterons, while the absorption on the carbon and beryllium impurities is about 15% – 20%, the direct electron damping via transit time magnetic pumping (TTMP) and electron Landau damping (ELD) takes around 10% and the mode converted power is estimated to be less than 5% of the total ICRF power.

3.3. Heating of the thermal plasma

The total power going to thermal ions and electrons, which includes the power transfer from the resonating deuterons via collisions as well as direct electron damping (TTMP/ELD), is shown in Fig. 4. As can be seen, the ion heating appears shortly after the RF-power is switched on whereas the electron heating is delayed. This can easily be understood since the ion heating occurs on the ion-ion collision time scale which is much shorter than the ion-electron collision time that characterises the collisional electron heating. Furthermore, the direct electron heating evolves as the electron temperature increases.

During most of the discharge the power flow to ions and electrons are comparable. This is consistent with the measured electron and ion temperatures, which are similar to each other. Both the ion and electron heating is concentrated in the centre, as can be seen in Fig. 5 displaying the volume integrated profiles of the ion and electron heating densities averaged over a sawtooth period. However, it should be noted that the calculated ion heating profile is somewhat broader than the electron heating profile. The reason for this is that the ion heating mainly occurs at lower power densities where the deuteron tail is less developed. Here, sawtooth redistribution plays a role to some extent. Firstly, it limits the tail formation, since fast deuterons which are expelled to regions with lower absorbed power densities effectively slow down more

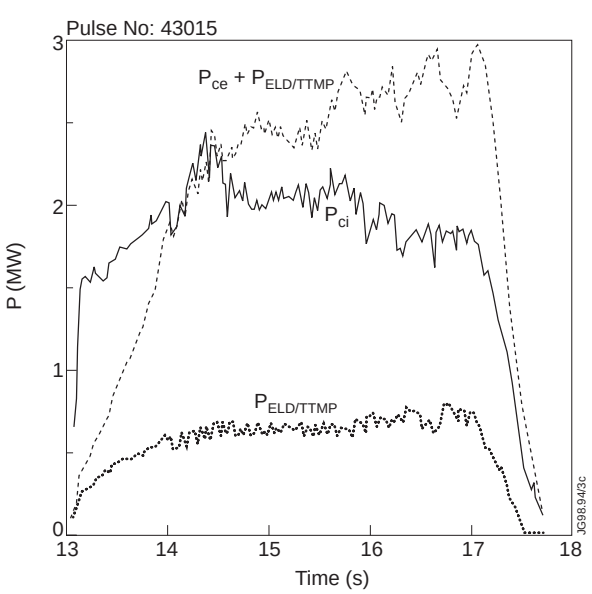

Fig. 4 Partition of power going to the thermal plasma via collision with fast deuterons and direct electron damping with sawtooth redistribution for the best performing discharge with $\omega = \omega_{cD}$ heating.

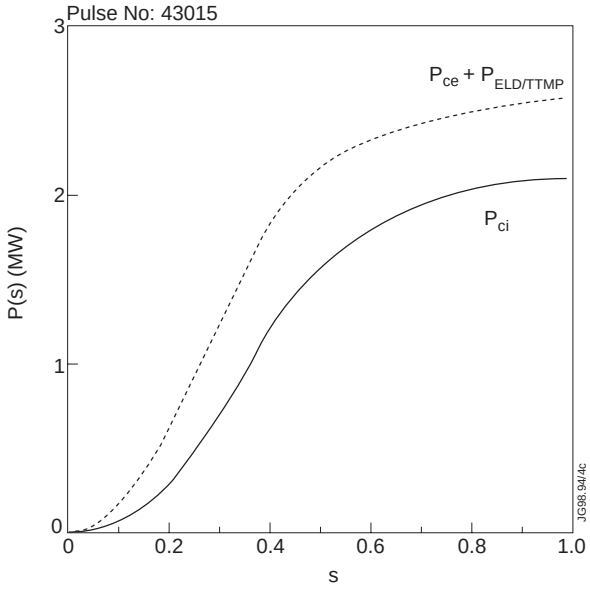

Fig. 5 Volume integrals of the power transfer densities to ions and electrons averaged over one sawtooth period, from t=14.84 s to 15.14 s, for the best performing discharge with $\omega = \omega_{cD}$ heating.

quickly. This lead to somewhat improved ion heating. The second effect is, of course, that the heating profiles, in particular the electron heating profile, broaden. The end result is that, when averaged over a sawtooth period, the differences between the ion and electron heating profiles are diminished.

3.4. Details of the deuteron distribution function

In the energy range of 100–450 keV PION calculations give a line-averaged deuteron tail temperature of about 110 keV within the normalised minor radius of r/a = 0.4. This tail temperature is in a reasonably good agreement with the tail temperature of 125±25 keV estimated from the neutron spectrometer [7]. The relatively low mean energy of the deuterons is consistent not only with the high non-thermal contribution of the D-T fusion reactivity but also with the fact that in the experiments no Toroidal Alfvén Eigenmodes (TAE) driven by ICRF-accelerated deuterons are observed [7]. Typically, the particle energies in the range of 500 keV are required to excite these modes [23].

3.5 Sensitivity analysis

The calculated neutron reactivity is sensitive both to the input data and to the calculated power deposition profile. To estimate the error bars on the calculated neutron rate due to uncertainties in the input data, a series of simulations were done where the background plasma parameters were varied within the experimental error bars. The error bars thus obtained should be compared to the error bar of about ±10% on the measured neutron rate. To evaluate the sensitivity of the neutron rate to the modelling of the power deposition, the power deposition profile used in the calculations was artificially modified.

We have considered the effect of varying the three most important input parameters on the calculated neutron rate, i.e. the electron temperature and density, which determine the slowing down time, and the deuteron concentration, which is an important parameter for the average energy of the resonating ions. The ion temperature, for example, plays a lesser role since the neutrons are mainly non-thermal. The experimental error bar on the deuteron concentration is about 10%, and also about 10% on the electron temperature and density. As these three parameters were varied within the error bars in the simulations, the neutron rate was affected by less than 10%.

To evaluate the sensitivity of the D-T fusion reactivity to the modelling of the power deposition profile, a series of simulations were done where the deuteron power deposition profile was artificially changed to have the form

$$p_{\mathrm{D}} = \frac{dP(s)}{ds} \Big/ \frac{dV}{ds}, \; P(s) = P(1)\frac{1-\exp[-(s-s_1)^2/s_0^2 \ln 2]}{1-\exp[-(1-s_1)^2/s_0^2 \ln 2]}, \qquad (1)$$

when $s \geq s_1$ and $P(s) = 0$ for $s < s_1$. Here, $s = \sqrt{\psi/\psi_a}$ is the flux surface co-ordinate, ψ is the poloidal flux, V is the plasma volume enclosed by the flux surface, $P(1)$ is the total absorbed power, s_0 is the width of the power deposition (it is almost the half width when $s_0 << 1$) and s_1 is chosen so that the modelled power deposition peaks at the same location as the power deposition calculated by the PION code.

The best agreement between the measured and calculated neutron rate is obtained when s_0 is between 0.2 and 0.3. When s_0 is increased, i.e. the power deposition made broader, the calculated neutron rate becomes progressively smaller than the measured one (e.g. 25% smaller for s_0 = 0.4). With a smaller value of s_0, on the other hand, a too peaked power deposition profile results in too strong variations in the simulated neutron rate after each sawtooth crash. The width of the deposition profile s_0 between 0.2 and 0.3 is consistent with the one calculated by the PION code, at t=15 s the half width is 0.27. Therefore, in view of the relatively small error bars due to variations in the background plasma parameters, the experimental power deposition profile cannot be very different from the one calculated by PION. The error bar on the calculated deposition width we estimate to be about 30%. It should of course also be said that it might possible to simulate the neutron rate with a power deposition which is quite different in shape as compared to the one calculated by PION. Since no direct information on the actual shape of the power deposition is available, we cannot rule out this possibility completely.

3.6 Dependence of the performance on the deuterium concentration

In general, good agreement between the measured and simulated neutron rate is found for discharges with similar deuterium concentrations (and electron densities) as the one in the best performing discharge discussed above. However, at higher deuterium concentrations (and lower electron densities) not as good agreement has been obtained.

A typical case with higher concentration is shown in Fig. 6 where an overview of discharge with a deuterium concentration of about 14% is shown. As can be seen, the neutron rate reaches a peak and then gradually decreases. It is not obvious from the data why the neutron rate decreases, and PION simulations do not replicate the time dependence of such discharges. In fact, when the deuteron concentration is higher than 10%, the discrepancy between PION calculations and measured neutron rates increases with concentration. One cannot explain the rollover of the neutron rate with a decreasing heating efficiency of the plasma since the diamagnetic plasma energy content and the H-mode factor with respect to the ITER89-P scaling law (H_{89} factor) [24] are not decreasing, Fig. 6, indicating that the power is well absorbed in the centre of the plasma throughout the discharge. The most likely explanation is then that some competing absorption mechanism, which absorbs the power in the centre of the plasma, starts to take a larger fraction of the power. In view of the dependence on the deuterium concentration, the prime candidate is mode conversion.

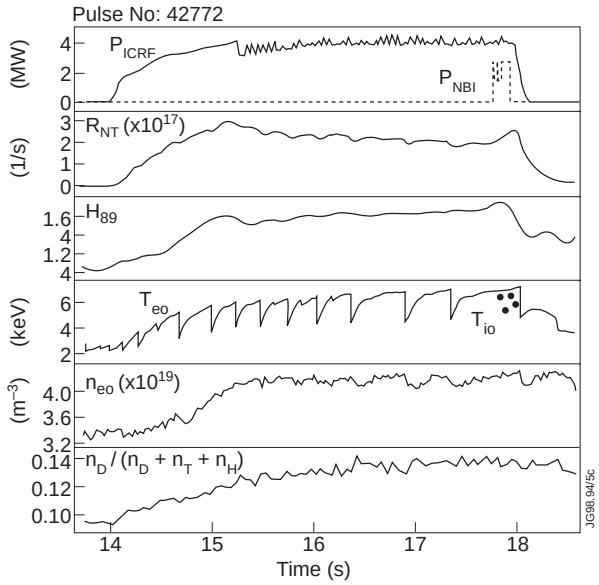

Fig. 6 An overview of a discharge with $\omega = \omega_{cD}$ and a high deuteron concentration.

The power required to be damped on the absorbing species from the fast wave, P_{req}, in order to match the neutron rate towards the end of the RF pulses have been estimated. In Fig. 7 the ratio P_{req} / P_{ICRF} shown as a function of the deuteron concentration. As can be seen, at concentrations greater than 20% only about 40% of the power needs to absorbed from the fast wave to explain the neutron rates, leaving 60% for possible mode conversion (or some other absorption mechanism).

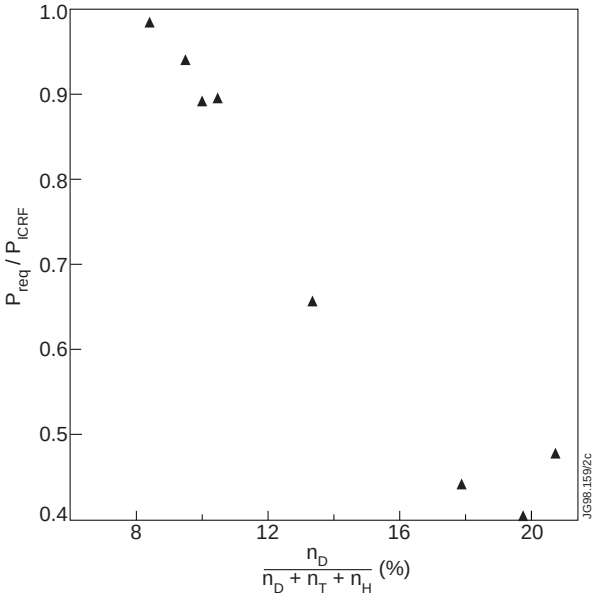

Fig. 7 Fraction of the total ICRF power that matches the measured D-T reaction rate in PION simulations for discharges with $\omega = \omega_{cD}$ heating as a function of the deuterium concentration.

As mentioned before, the simple Budden formula is used in PION to estimate the amount of mode converted power. However, the amount of power estimated to be mode converted with this formula is not enough to explain the experimental results. For the

discharges with concentrations in the region of 20%, the estimated fraction of mode converted power is 10 – 20 %, i.e. too little to explain the results in Fig. 7. Of course, there are large uncertainties in the estimation of the deuteron concentration and the amount of carbon and beryllium impurities in the centre. Both these quantities play an important role for the mode conversion and it is possible that more accurate information on the concentrations could explain the experimental results even with the Budden formula. Nevertheless, since analysis of mode conversion in a toroidal geometry is very difficult, and it is only with some recently developed full wave codes e.g. [25] that analysis might be possible (restriction on the grid size might be a problem), we have to leave this issue to a future investigation.

To conclude the discussion on fundamental deuterium heating, we can say that PION simulations are in good agreement with experimental results for moderate deuterium concentrations. However, at high concentrations where mode conversion, which is not properly treated in PION, should play an important role, discrepancies start to appear.)

4. ANALYSIS OF DISCHARGES WITH SECOND HARMONIC TRITIUM RESONANCE

During the D-T campaign on JET two types of discharges with the second harmonic tritium resonance in the plasma centre were tested, i.e. discharges with and without ^{3}He gas puff. Since the fundamental ^{3}He resonance coincides with the second harmonic tritium resonance, ^{3}He absorption in the discharges with ^{3}He gas puff was expected to be significant. In the experiments major differences between the two discharge types were indeed observed, as shown in Fig. 8. In the following we will discuss these observations in detail.

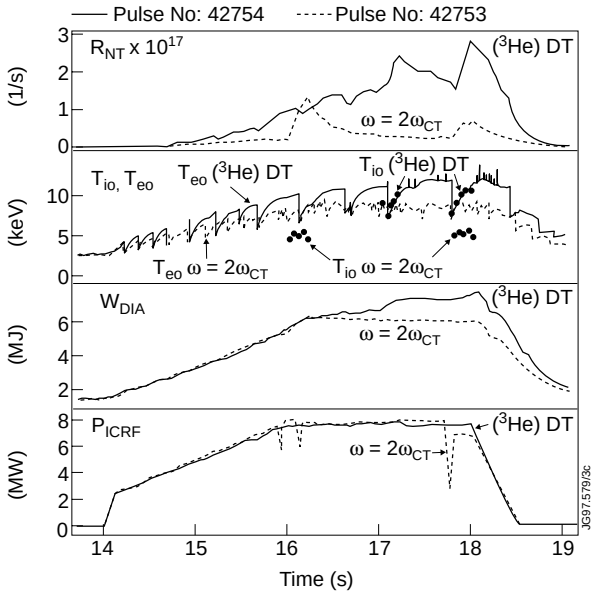

Fig. 8 An overview of two $\omega = 2\omega_{cT} = \omega_{^3He}$ discharges, one with and one without ^{3}He gas puff.

4.1 Pure ω=2ω_{cT} heating

The experimental results with the pure $\omega = 2\omega_{cT}$ heating (no ^{3}He gas puff) on JET are consistent with the theoretical expectations described in Sec. 1. The D-T fusion reaction rate in the pure $\omega = 2\omega_{cT}$ scenario was about an order of magnitude lower than in the $\omega = \omega_{cD}$ scenario. Furthermore, the ion temperature was significantly lower than the electron temperature, indicating less effective ion heating.

4.1.a. Simulation of the neutron rate

A comparison between simulated and measured neutron yields for $\omega = 2\omega_{cT}$ heating is shown in Fig. 9, including a simulation in which the ICRF power has been set to zero to assess the effects of NBI blips. As can be seen, the agreement is very good, with about 20% of non-thermal neutrons according to the calculations. Three diagnostic tritium beam blips were applied in the discharge: the first between t=16.0 s and t=16.2 s; the second between t=17.8 s and t=17.915 s; and the third between t=17.95 s and t=18.0 s. Good agreement between the measured and calculated D-T fusion reaction rate during the diagnostic tritium beam blips indicates that the slowing down of the injected and ICRF heated tritons is classical.

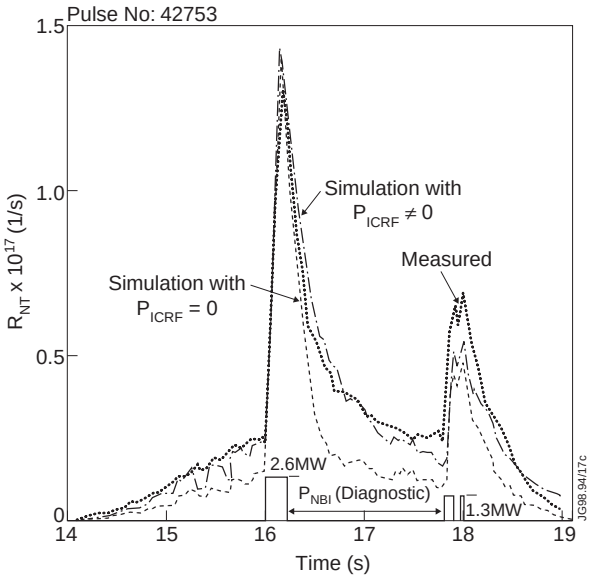

Fig. 9 Simulated and measured D-T fusion reaction rate for $\omega = 2\omega_{cT}$ heating. The simulated thermal component includes also the reactions between beam injected tritons and thermal deuterons.

4.1.b. Power partition

The power partition between the main absorbing species, the tritium ions and electrons (ELD/TTMP), is shown in Fig. 10. In the beginning of the simulation tritons absorb about 25% of the total ICRF power. Towards the end of the discharge when the ion temperature is higher and a tail on the tritium distribution has developed, the triton absorption increases to about 45%. If the tail on the tritium distribution function is not taken into account, the triton absorption stays at about 10% of the total ICRF power. This clearly shows the importance of including the effect of the high energy tail in the power deposition calculation. Furthermore, the simulation suggests that during the high-power phase about 1 MW of power is lost by energetic tritons intersecting the wall, which is consistent with the relatively low H_{89} factor.

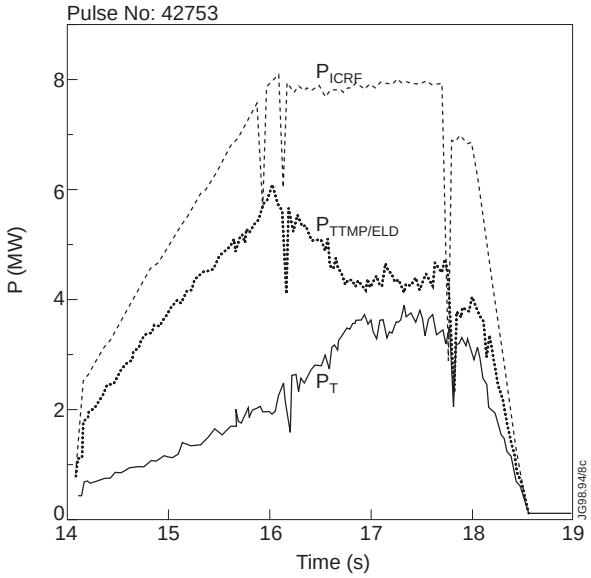

Fig. 10 Partition of the absorbed RF-power for $\omega = 2\omega_{cT}$.

4.1.c. Heating of the thermal plasma

The total power going the thermal ions and electrons is shown in Fig. 11. As expected the electron heating dominates, mainly due to the large fraction of direct electron heating. This is

consistent with the measured electron temperature being considerably higher than the ion temperature. The profiles of the volume integrated power densities to the thermal ions and electrons are discussed and compared to a case with ^{3}He gas puff in section 4.2.b.

4.1.d. Sensitivity analysis

Since most of the calculated neutron rate is thermal, the greatest uncertainty in the simulations of the neutron rate for the $\omega = 2\omega_{cT}$ discharges is in the ion temperature, T_i. The thermal reactivity scales approximately as $\sim T_i^3$ in the relevant temperature range. Thus, with an experimental error bar of 10% on T_i, the error in the calculated neutron rate is about 25–30%. Consequently, we cannot say within the error bars, except during and after the beam blips, whether there is a non-thermal component in the measured neutron rate. However, the fact that the tritons injected during the beam blips absorb RF-power, and that the neutron rate is well simulated during that phase of the discharge indicate that the modelling is reasonably correct. Furthermore, there is independent experimental evidence for the existence of a triton tail from observations of TAE mode activity and high energy NPA measurements [7].

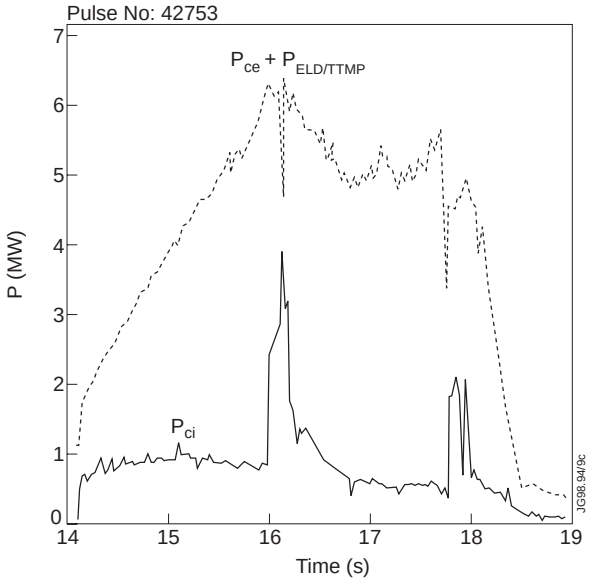

Fig. 11 Partition of power going to the thermal plasma via collisions with fast tritons and direct electron heating for $\omega = 2\omega_{cT}$.

Another uncertainty concerns the amount of ^{3}He in the discharge. As pointed out in Ref. [26], there is always a small amount of ^{3}He mixed in with the tritium owing to radio-active decay of the tritium. Even relatively small amounts, ~0.5%, of ^{3}He can according to the simulations absorb a significant fraction of the power. However, the agreement between the measured and simulated neutron rate deteriorates somewhat when we include such small amounts of ^{3}He in the simulations.

4.2 Discharges with ^{3}He gas puff

When a few percent of ^{3}He was added in the experiments, much higher ion temperatures were achieved and the H_{89} factor was improved, as is shown in Fig. 8. Here, ^{3}He is puffed in to the discharge before the main ICRH heating phase at t=13.5 s. In particular, note the high central ion temperature which exceeds the electron temperature in the plasma centre.

4.2.a. Power partition

Figure 12 shows the power partition among the main species given by PION for discharge with ^{3}He gas puff in Fig. 8. In the steady stage of the discharge the simulations suggest that the ^{3}He ions absorb most of the power (up to 90%), and the rest goes mainly to direct electron damping.

The power absorbed by tritons is very small, and the calculations suggest that the contribution to the neutron yield is negligible. In fact, the measured neutron rate is consistent with being purely thermal.

4.2.b. Heating of the thermal plasma

The high critical velocity of the ^{3}He ions, together with the fact that ^{3}He ions are accelerated more uniformly in velocity space, leads to good ion heating. The profiles of the volume integrated thermal ion and electron heating power densities, averaged over a sawtooth period, are shown in Fig. 13 for the pure $\omega = 2\omega_{cT}$ discharge and the combined discharge. As can be seen, the ion heating is much better and more central in the case when a few percent ^{3}He is included. This is consistent with the observed electron and ion temperatures.

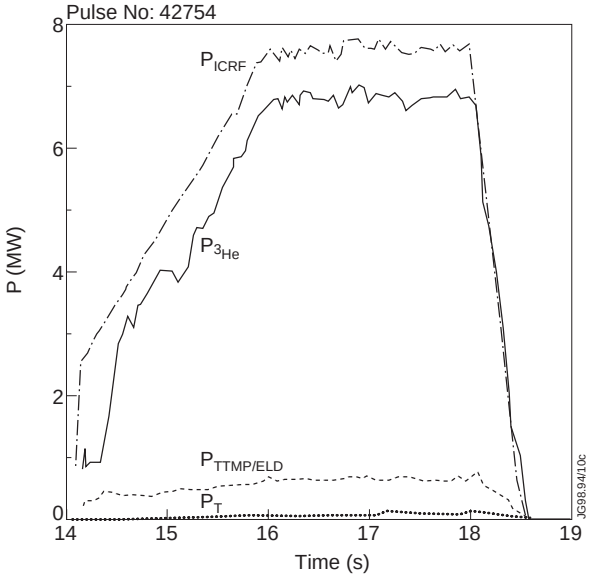

Fig. 12 Partition of the absorbed RF-power for $\omega = 2\omega_{cT} = \omega_{^3He}$ with ^{3}He gas puff.

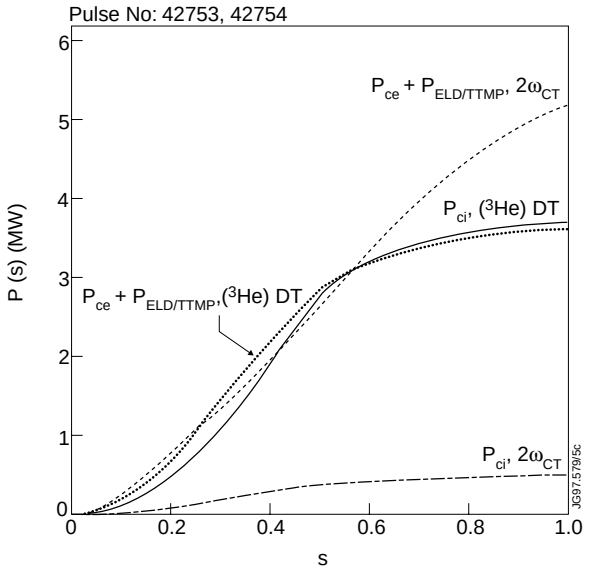

Fig. 13 Volume integrals of the power transfer densities to ions and electrons averaged over one sawtooth period for $\omega = 2\omega_{cT} = \omega_{^3He}$ discharges, one with and one without ^{3}He gas puff.

In heating a reactor to ignition a large fraction of ion heating gives greater freedom in choosing the route to ignition [9]. The results presented here suggest that by injecting a small amount of ^{3}He in the start up phase the ion heating can be improved. Once the plasma is hot and dense enough, the second harmonic tritium heating can take over and will then also give rise to mainly ion heating since the critical velocity increases due to the higher electron temperature.

4.2.c. Simulation of the diamagnetic energy content

Since the calculated non-thermal neutron yield is very small, it cannot be used to diagnose if the simulation is consistent with the experimental results. Instead, we have compared the measured diamagnetic stored energy content with the calculated one, Fig. 14. Since this quantity measures the perpendicular energy of the plasma, the contribution from fast RF-accelerated ions which have most of their energy in the perpendicular direction can be significant. As can be seen in

Fig. 14, the agreement between the measurement and simulation is rather good and the contribution from the fast ions is relatively large.

The error bars on the calculated contribution from the fast ions can easily be estimated since the fast ion energy content is approximately proportional to $P_{\mathrm{ICRF}} t_{\mathrm{s}} \sim P_{\mathrm{ICRF}} T_{\mathrm{e}}^{3/2} / n_{\mathrm{e}}$. Thus, a 10% error bar on the electron temperature T_{e} and the electron density n_{e} gives rise to an error bar of about 25–30% . The total error bar, including the thermal contribution, is estimated to be about 25%. In spite of the relatively large error bar, the good agreement with the time evolution of the measured diamagnetic stored energy is an indication that the simulation is consistent with the experimental results.

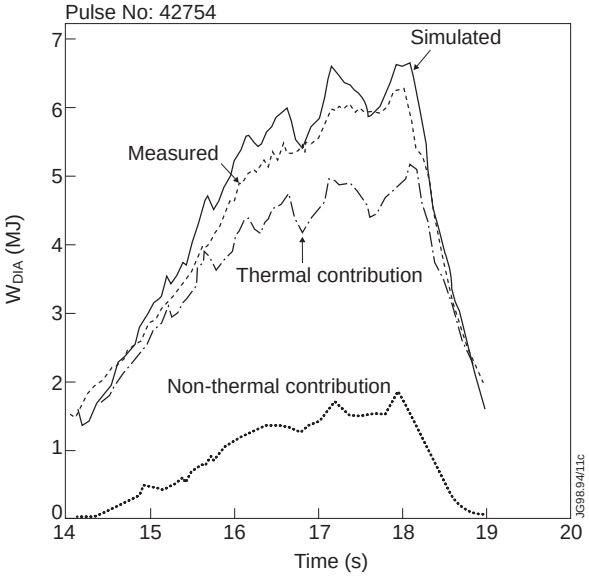

Fig. 14 Comparison between measured and simulated diamagnetic stored energy for a $\omega = 2\omega_{\mathrm{cT}} = \omega_{^3\mathrm{He}}$ *discharge with* ^{3}*He gas puff.*

5. ANALYSIS OF SECOND HARMONIC HEATING OF DEUTERIUM

The final scenario we have analysed is second harmonic heating of deuterium. However, owing to small amounts of residual hydrogen, there is always a concomitant fundamental minority heating of hydrogen. In fact, in most cases the absorption on the hydrogen dominates and the enhancement of the neutron rate due to non-thermal deuterons is limited. There is an advantage with having a few percent of hydrogen in the discharge, since the single pass absorption becomes very strong. On the other hand, the drawback is that the ion heating tends to be modest, owing to the fact that the absorbing hydrogen ions often are accelerated to very high energies.

To simulate discharges with second harmonic deuterium heating is intricate since the partition of the absorbed RF-power depends sensitively on the concentration of hydrogen. However, one can turn the problem around and use the calculations to find out which hydrogen concentration is consistent with the measured neutron rate and the measured diamagnetic stored energy. An overview of a discharge for which such an analysis has been carried out is given in Fig. 15.

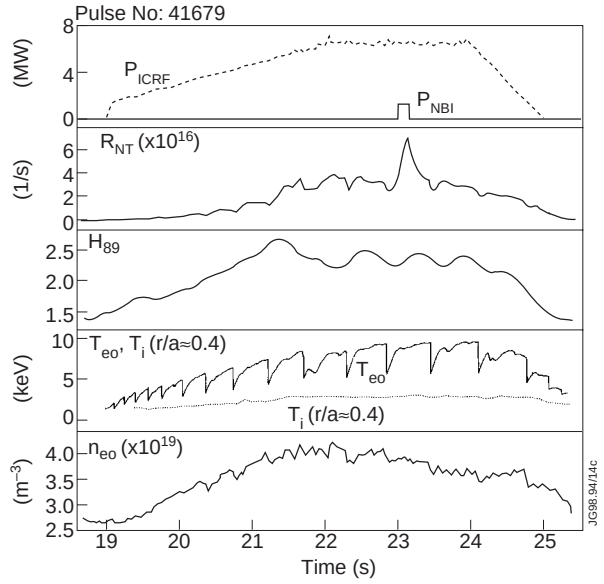

Fig. 15 Overview of a $\omega = 2\omega_{\mathrm{cD}} = \omega_{\mathrm{cH}}$ *discharge.*

5.1 Neutron rate and diamagnetic stored energy

In Fig. 16 a comparison of measured and simulated neutron rates is shown together with of the calculated thermal contribution. In the simulation a hydrogen concentration of $n_H/(n_H + n_D + n_T) = 3\%$ has been assumed. With this concentration the measured neutron rate can be simulated quite well, and the non-thermal contribution is fairly high. The hydrogen concentration measured with the D_α, H_α and T_α signals, which are weighted towards the plasma edge, is about 1.7%. Thus, we have to assume a somewhat higher hydrogen concentration in the centre than is estimated at the plasma edge to obtain consistency with the measured neutron rate.

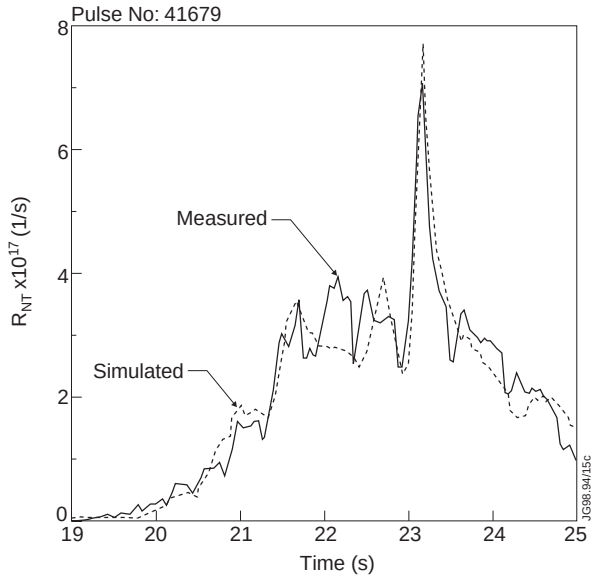

Fig. 16 Comparison between measured and simulated D-T neutron rate for a $\omega = 2\omega_{cD} = \omega_{cH}$ discharge assuming $n_H/(n_H + n_D + n_T) = 3\%$.

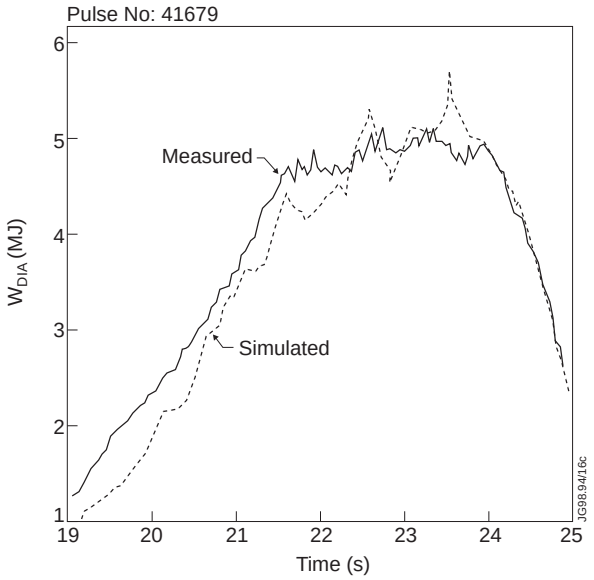

Fig. 17 Comparison between measured and simulated diamagnetic stored energy for a $\omega = 2\omega_{cD} = \omega_{cH}$ discharge assuming $n_H/(n_H + n_D + n_T) = 3\%$.

With this concentration good agreement between the simulations and the measured diamagnetic stored energy is also found, Fig. 17. This further indicates that the power partition between the hydrogen and deuterium is about right.

5.2 Power partition

The power partition among the main resonating species is shown in Fig. 18. The hydrogen absorption is the dominating absorption mechanism and the power going to second harmonic deuterium heating is just above 1 MW. It is interesting to note that even this small deuterium absorption is enough to give rise to a significant non-thermal contribution to the neutron rate.

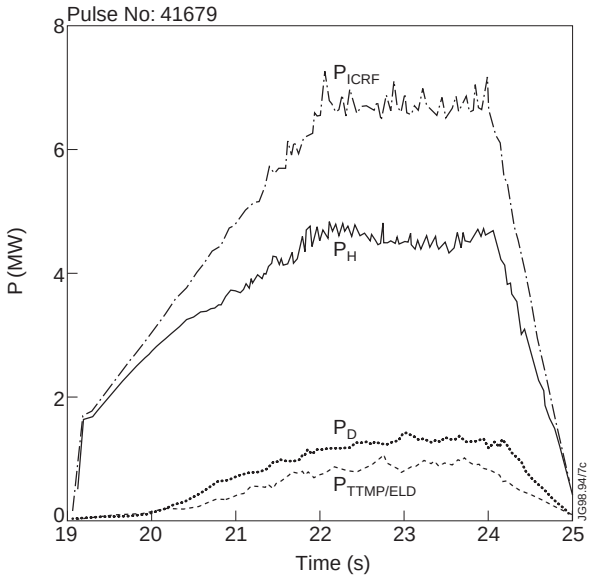

Fig. 18 Partition of the absorbed RF-power for a $\omega = 2\omega_{cD} = \omega_{cH}$ discharge assuming $n_H/(n_H + n_D + n_T) = 3\%$.

5.3 Heating of the thermal plasma

The heating powers going to thermal ions and electrons are shown in Fig. 19. As expected, mainly the electrons are heated in this scenario. This result can be contrasted with the effect of having a few percent of ^{3}He in the second harmonic tritium scenario, which gave rise to a significant amount of ion heating. The problem of dominating bulk electron heating in the $\omega = 2\omega_{cD} = \omega_{cH}$ will persist also in ITER, especially in the start up phase. The second harmonic deuterium scenario is therefore not ideal for bringing ITER to ignition.

In Fig. 20 the power densities going to the thermal ions and electrons via collisions are shown for two simulations. In one simulation finite orbit width effects are taken into account, while in the other the zero banana width limit has been assumed. As can be seen, the collisional transfer to the electrons is strongly affected, whereas the power density to the ions is almost unaffected. The reason is of course that the power to the electrons is transferred by high energy ions with wide orbits while the power going to the ions comes mainly from resonating ions with energies below the critical energy, i.e. ions with small orbit width.

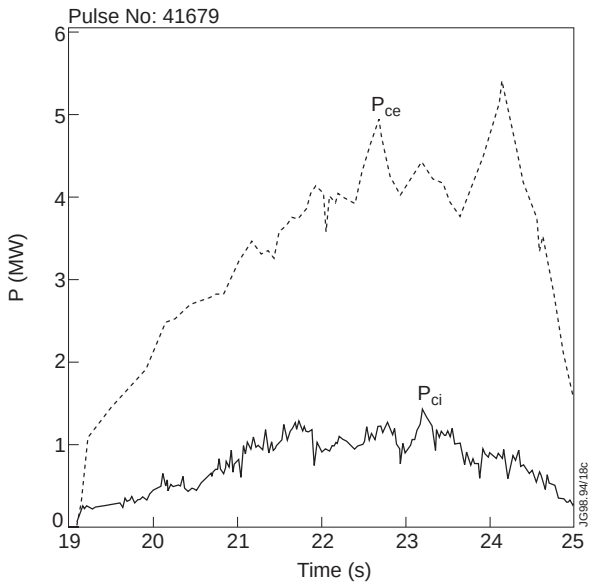

Fig. 19 Partition of power going to the thermal plasma via collision and direct electron damping a $\omega = 2\omega_{cD} = \omega_{cH}$ discharge assuming $n_H/(n_H + n_D + n_T) = 3\%$.

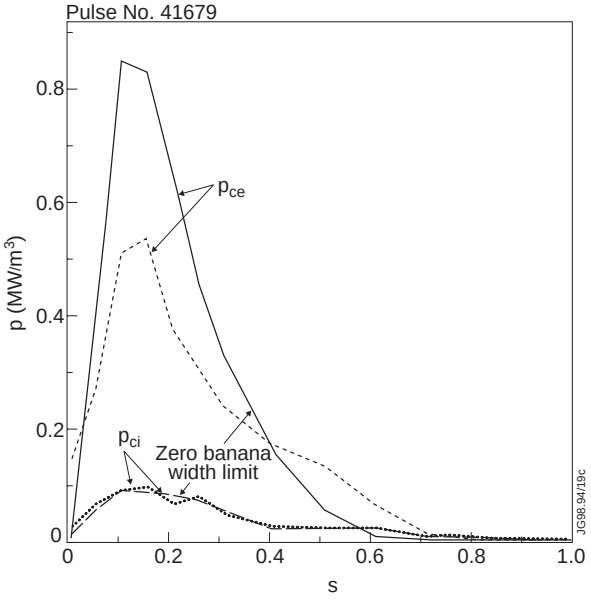

Fig. 20 Collisional power densities to the thermal ions and electrons with and without finite orbit width effects taken into account at t=22 s.

5.4 Sensitivity analysis

We have studied the sensitivity of the simulation results with respect to parameters we consider most important, i.e. the modelled ion temperature profile and the hydrogen concentration. In this particular discharge the ion temperature profile was not measured; only the ion temperature measurement at $r/a \approx 0.4$ with an X-ray crystal spectrometer is available. In the simulations the ion temperature profile has therefore been assumed to be the same as that of electrons, and it has

been scaled to agree with the ion temperature measurement at $r/a \approx 0.4$. The uncertainty thus introduced on the neutron rate and the diamagnetic plasma energy content has been studied by comparing the results with simulations where the ion temperature has been assumed to be in the form $T_i \propto [1-0.9(r/a)^2]^{\alpha}$. This analysis indicates that while the modelled ion temperature profile corresponds to $\alpha \approx 1$, both the total neutron rate and the diamagnetic energy content vary only by 20% when α is varied between 0.2 and 2.

The simulation results have been found to depend more sensitively on the assumed hydrogen concentration, since it determines to a large extent the partition of the power between hydrogen ions and deuterons. For example, if the hydrogen concentration is assumed to be 1% instead of the 3% used to obtain consistency with the neutrons, the RF power absorbed on the deuterons is doubled. As a result, the neutron rate is overestimated by almost a factor of two. Furthermore, the agreement with the diamagnetic stored energy deteriorates, it being overestimated by up to 0.8 MJ. It should also be noted that we cannot obtain consistency between the simulation results and the measurements by assuming a hydrogen concentration of 1.7% and a lower heating efficiency. In such a simulation the neutron rate can be matched, but the diamagnetic stored energy is underestimated.

In the view of relatively small error bar on the total neutron rate and diamagnetic plasma energy content due to the modelled ion temperature, we are inclined to conclude that the hydrogen concentration in the PION simulations needs to somewhat higher than the one measured near the plasma edge to obtain consistency with the experiments. It is of course quite likely that the hydrogen concentration varies over the plasma radius, but it might also be appropriate to investigate other possibilities.

6. SUMMARY AND DISCUSSION

A number of ICRF heating scenarios with relevance for a reactor were tested in the recent D-T campaign at JET. We have analysed most of these by comparing experimental results with code simulations. In JET the most attractive scenario was deuterium minority heating. As predicted by PION code simulations, this scenario provided good ion heating and a high non-thermal neutron rate. Another possibility for absorbing power on the deuterons is to use second harmonic deuterium heating. However, owing to residual hydrogen, a large fraction of the power is absorbed through hydrogen minority heating. Furthermore, because of the low critical energy for hydrogen, most of the power absorbed by the hydrogen ions is collisionally transferred to the electrons, i.e. the ion heating tends to be modest in this scenario.

The second harmonic tritium scenario, which is relevant for operation of a reactor with a 50:50 D-T mixture, did not perform as well as the deuterium minority scenario in JET. According to the calculations there are two main reasons for this. Firstly, the competition from direct electron heating was strong and a relatively small fraction of the power was absorbed by the tritons. Secondly, the tail developing on the tritium distribution function extended to too high

energies (i.e. energies above the critical energy). By adding a few percent of ^{3}He, the ion heating was greatly improved. PION code simulations suggest that the reason for this was predominant absorption of the wave power by the ^{3}He ions ($\omega = \omega_{c^3He} = 2\omega_{cT}$). The accelerated ^{3}He ions heat ions efficiently because they have a high critical energy and the tail formation normally is moderate. One can envisage using heating at $\omega = \omega_{c^3He} = 2\omega_{cT}$ in a reactor with a small concentration of ^{3}He in the beginning of the discharge. Later during the start-up, when ^{3}He diffuses out and higher temperatures and densities are reached, damping on tritons can take over. However, it should also be noted that PION simulations carried out for ITER suggest that pure $\omega = 2\omega_{cT}$ can provide adequate ion heating in ITER if an appropriate path to ignition is followed [9].

In the simulations with the PION code a variety of effects played an important role. For scenarios like second harmonic tritium heating the absorption depends strongly on the distribution function of the resonating ions and there is a strong competition from other absorbing species. The influence of the velocity distribution on the power deposition was therefore significant. Finite orbit width effects were also found to be important. This was especially the case for the $\omega = 2\omega_{cT}$ scenario, where losses due to orbits intersecting the wall were notable. As was evident from deuterium minority heating, sawtooth redistribution of fast ions played a significant role. In particular, the profiles of the power densities going to heating of the thermal plasma, when averaged over a sawtooth period, were broadened.

The physics on which the PION code is based seems sufficient for describing the global behaviour of ICRF related quantities in most cases for the ICRF heating scenarios tested in the recent D-T campaign at JET. This increases confidence in theoretical modelling of ICRF heating in future experiments. However, one cannot completely rule out the possibility that power depositions with shapes quite different from the ones calculated by PION could explain the measurements. This must be kept in mind when making predictions for future machines. Furthermore, for cases where the modelling in PION is questionable, in particular for high minority concentrations where mode conversion is important, the calculations are not consistent with the experimental results. Improved modelling, involving codes which treat mode conversion properly in a toroidal geometry, is therefore required in order to analyse scenarios with high minority concentration. However, this might not be necessary for analysis of high concentration deuterium minority heating in a reactor where the single pass absorption on deuterons is expected to be quite strong and a comparatively small fraction of power is left for possible mode conversion [27]. In the relatively attractive scenario with combined ^{3}He minority heating and second harmonic heating one would not like to use too high ^{3}He concentrations because of the dilution, and the physics which PION is based on should be adequate for analysing this scenario in a reactor. Furthermore, the pure $\omega = 2\omega_{cT}$ should also be well described by the PION code.

REFERENCES

[1] Bosia, G., *et al.*, Proceedings of the 16th IAEA Conference on Fusion Energy, Montreal, 1996, Vol. 2, p. 917.

[2] Phillips, C.K., *et al.*, Phys. Plasmas **2** 2427 (1995).

[3] McGuire, K.M., *et al.*, Phys. Plasmas **2** 2176 (1995).

[4] Gormezano, C., *et al.*, Phys. Rev. Lett. **80** 5544 (1998)

[5] Keilhacker, M., *et al.*, "High Fusion Performance from Deuterium-Tritium Plasmas in JET," to be published in Nuclear Fusion.

[6] Start, D.F.H., *et al.*, "Bulk Ion Heating with ICRH in JET D-T Plasmas," to be published in Nuclear Fusion.

[7] Start, D.F.H., *et al.*, Phys. Rev. Lett. **80** 4681 (1998)

[8] Stix T.H., Nuclear Fusion **15** 737 (1975).

[9] Start, D.F.H., *et al.*, 24th European Physical Society Conference on Controlled Fusion and Plasma Physics, Berchtesgaden 9–13 June 1997, Europhysics Conference Abstracts Vol. **21A,** Part I, 141–144.

[10] Llobet, X., Hellsten, T., Villard, L., in Theory of Fusion Plasmas (Proc. Varenna-Lausanne Int. Workshop Chexbres, 1988), Editrice Compositori, Bologna (1988) 663.

[11] Edery, P., Picq, H., Samain, A., and Gambier, D.J., "*Numerical Modelisation of RF Waves in the Ion Cyclotron Range of Frequencies for Tokamak Plasmas*," Report EUR-CEA-FC-1334, Association Euratom-CEA. St. Paul lez Durances (1987).

[12] Kerbel, G.D., and McCoy, M. G., Phys. Fluids **28** 3629 (1985).

[13] Carlsson, J., Hellsten, T., and Eriksson, L.-G., *"Fido, a code for computing the resonant-ion distribution function during ICRH,"* Royal Institute of Technology, Report ALF-1996-104, Stockholm (1996).

[14] Eriksson, L.-G., Hellsten, T., and Willén, U., Nuclear Fusion **33** 1037 (1993).

[15] Eriksson, L.-G., and Hellsten, T., Physica Scripta **55** 70 (1995).

[16] Eriksson, L.-G., *et al.*, Nuclear Fusion **38** 265 (1998).

[17] Hellsten, T., and Villard, L., Nuclear Fusion **28** 285 (1988).

[18] Hellsten, T., and Eriksson, L.-G., Nuclear Fusion **29** 2165 (1989).

[19] Budden, K.G., in Radio Waves in the Ionosphere (Cambridge University Press, Cambridge, 1961).

[20] Anderson, D., *et al.*, Plasma Phys. Controlled Fusion **29** 891 (1987).

[21] Anderson, D., *et al.*, Nuclear Fusion **34** 217 (1994).

[22] Mantsinen, M.J., *et al.*, 24th European Physical Society Conference on Controlled Fusion and Plasma Physics, Berchtesgaden 9–13 June 1997, Europhysics Conference Abstracts Vol. **21A,** Part I, 137–140.

[23] Borba, D., *et al.*, "Alfvén Eigenmode Stability and Fast Particle Transport in JET," to appear in the Proceedings of the 5th IAEA Technical Committee Meeting on Alpha Parti-

cles in Fusion Research, 8–11 September, 1997, JET, UK.
[24] Yushmanov, P.N., *et al.*, Nuclear Fusion **30**, 1999 (1990).
[25] Jaun, A., *et al.*, Computer Phys. Communications **92** 153 (1995).
[26] Bhatnagar, V.P., *et al.*, 2nd Europhysics Topical Conference on Radio Frequency Heating and Current Drive of Fusion Devices, Brussels, Belgium, 20–23 January 1998, Europhysics Conference Abstracts Vol. **22A** pp 29–32, Eds Jacquinot, J., Van Oost, G., Weynants, R.R.
[27] Bhatnagar, V.P., *et al.*, Nuclear Fusion **33** (1993) 83.